Antiferromagnetic three-sublattice Tb ordering in $Tb_{14}Ag_{51}$

P. Fischer,[1,*] V. Pomjakushin,[1] L. Keller,[1] A. Daoud-Aladine,[1] W. Sikora,[2] A. Dommann,[3,†] and F. Hulliger[3]
[1]*Laboratory for Neutron Scattering, ETH Zurich & Paul Scherrer Institute, CH-5232 Villigen PSI, Switzerland*
[2]*Faculty of Physics and Applied Computer Science, AGH University of Science and Technology, PL-30-059 Krakow, Poland*
[3]*Laboratory for Solid State Physics, ETH Hönggerberg, CH-8093 Zurich, Switzerland*
(Received 23 March 2005; revised manuscript received 16 May 2005; published 12 October 2005)

Bulk magnetic, x-ray, and neutron-diffraction measurements were performed on polycrystalline $Tb_{14}Ag_{51}$ in the temperature range from 1.5 K to room temperature. Its chemical $Gd_{14}Ag_{51}$-type structure corresponding to space group $P6/m$ has been refined at 300 and at 30 K. Combined with group-theoretical symmetry analysis, we show that the magnetic structure of this intermetallic compound is of a different $\mathbf{k}=(1/3,1/3,0)$ type with three magnetic Tb sublattices ordering simultaneously below $T_N=27.5(5)$ K according to the combined irreducible representations τ_4 and τ_6.

DOI: 10.1103/PhysRevB.72.134413 PACS number(s): 75.25.+z, 61.12.Ld, 71.20.Eh

I. INTRODUCTION

Intermetallic uranium and rare-earth $A_{14}B_{51}$ compounds with $Gd_{14}Ag_{51}$ structure[1] have interesting physical properties such as coexistence of antiferromagnetic order and heavy-fermion behavior in $Ce_{14}X_{51}$ (X=Au,Ag,Cu),[2] and in $U_{14}Au_{51}$.[3–5] This is related to the fact that there are three crystallographically distinct A sites in this structure.

Moreover, its particular hexagonal symmetry, due to quasitriangular arrangement of magnetic ions, gives rise to considerable geometric frustrations in the magnetic interactions. Thus from bulk physical measurements[2] it was concluded that generally not all Ce sublattices order magnetically in the antiferromagnetic $Ce_{14}X_{51}$ compounds with Néel temperatures $T_N \leqslant 3.2$ K. Also in $U_{14}Au_{51}$ with $T_N=22$ K the $(2e)$ sites do not exhibit magnetic ordering.

In 1997 the correct antiferromagnetic structure of this compound had been established by Brown *et al.* from single-crystal neutron polarimetric and unpolarized neutron-diffraction measurements[4] and had been later confirmed by muon spin-rotation (μSR) investigations performed by Schenck *et al.*[5] The $k=0$ magnetic structure was found to be noncollinear according to the Shubnikov group $P6/m'$ with the U moments confined to the (a,b) plane. The moments of U atoms in each of the two sets of sixfold sites are arranged hexagonally with rotations of 60° between them and the two sets rotated with respect to one another by 50°.

The above-mentioned interesting magnetic properties motivated us to start powder x-ray and neutron-diffraction investigations as well as bulk magnetic measurements on the similar antiferromagnetic rare-earth compound $Tb_{14}Ag_{51}$ in order to determine to which extent magnetic ordering is different and in particular to investigate whether there may be also magnetic order on all rare-earth sites. Because of the larger magnetic Tb moments powder neutron diffraction is more appropriate to obtain first information on magnetic ordering than in $U_{14}Au_{51}$,[3] with rather small magnetic U moments and $k=0$ magnetic structure. Indeed neutron-diffraction experiments performed by Dommann *et al.*[6] revealed $\mathbf{k}=(1/3,1/3,0)$ in the case of $Tb_{14}Ag_{51}$. In the present work we obtained considerably improved neutron-diffraction data and performed a careful analysis of both the chemical and magnetic structures of $Tb_{14}Ag_{51}$. In particular we shall prove that in $Tb_{14}Ag_{51}$ the magnetic ordering is of a different type in the important class of intermetallic $A_{14}B_{51}$ compounds with remarkable variation of physical properties. In contrast to the heavy fermion system $U_{14}Au_{51}$,[4] in $Tb_{14}Ag_{51}$ all three A sublattices are shown to order magnetically below $T_N=27.5(5)$ K.

We also measured zero-field μSR spectra of the powder sample of $Tb_{14}Ag_{51}$ at the GPS spectrometer of Paul Scherrer Institute at 5, 20, and at 30 K. Unfortunately, in contrast to $U_{14}Au_{51}$,[5] they do not provide much additional information on the magnetic Tb ordering, either because of the large magnetic Tb moments, the different kind of magnetic ordering, and/or magnetic frustration effects. Therefore we do not include these μSR results in the present work.

II. EXPERIMENT

Polycrystalline samples of $Tb_{14}Ag_{51}$ were prepared in a similar way as described for $U_{14}Au_{51}$ in Ref. 7. Under the microscope the specimens appeared to be single-phase materials. Also no lines due to foreign phases were detectable on the x-ray-diffraction patterns. The measured magnetic susceptibility of the sample is illustrated in Fig. 1. It exhibits a strong peak at 27.9 K, indicating antiferromagnetic ordering. The measured effective magnetic moment $p_{obs}=9.67\mu_B$/Tb was found to be close to the free ion value $p_{cal}=9.72\mu_B$/Tb of Tb^{3+} with $^7F_6$ ground state. The observed value had been determined from the slope of the straight line of the corresponding inverse magnetic susceptibility. Specific-heat data also revealed a small anomaly at 27 K.

Neutron-diffraction investigations[6] were initially performed on diffractometer DMC at the reactor Saphir at temperatures $T=30$ and 1.6 K (scattering angle range 3° to 82.9°, step 0.1°) and short measurements also during cooling, using the neutron wavelength $\lambda=1.7$ Å. For these measurements the sample was enclosed under He gas atmosphere into a cylindrical V container of diameter 8 mm and approximately 5 cm height and had been mounted into an ILL-type cryostat. From transmission measurements the product of

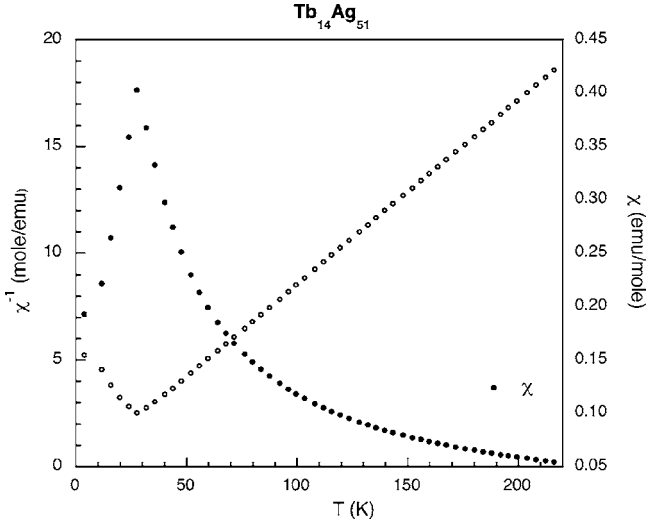

FIG. 1. Temperature dependences of magnetic susceptibility and of its inverse of polycrystalline $Tb_{14}Ag_{51}$, determined in an external magnetic field of 4.67 kOe.

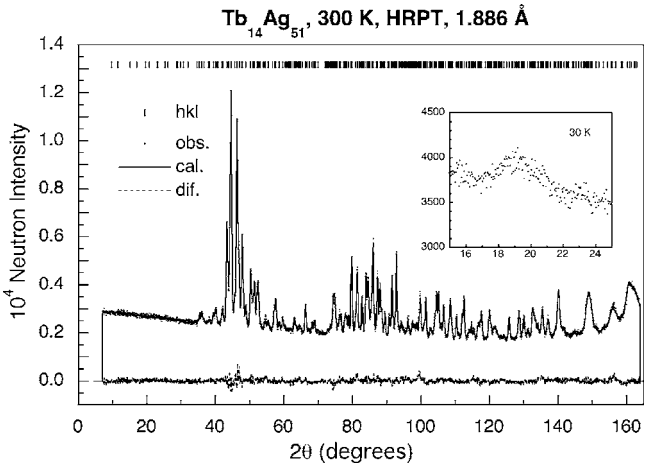

FIG. 2. Observed (points), calculated (line) and difference (obs.-cal., dashed) neutron-diffraction pattern of $Tb_{14}Ag_{51}$ at 300 K in the paramagnetic state (measured without cryostat). Note the strong paramagnetic contribution to the background at low scattering angles. The inset illustrates the dominant broad peak associated with short-range magnetic order at 30 K.

linear absorption coefficient μ and sample radius r had been determined as 0.698.

Recently more extended and more precise neutron-diffraction measurements were made on the same sample (enclosed in a cylindrical V tube of 9 mm diameter and about 4 cm sample height, under He gas atmosphere) on diffractometers DMC (Ref. 8) and HRPT,[9] situated at the Swiss spallation neutron source SINQ of Paul Scherrer Institute at Villigen. The high intensity mode (i.e., without primary Soller collimation) and neutron wavelengths $\lambda=2.567$ and 1.886 Å were used, respectively, on these instruments. Temperatures in the range from 1.5 to 300 K were attained by means of an ILL-type He flow cryostat. Because of the presence of rather large grains of the hard material, sample oscillation had been used in the final 1.5- and 30-K measurements on HRPT and DMC in order to improve powder averaging. Recent transmission measurements on the sample yielded for $\lambda=1.886$ Å $\mu r=0.801$. The data were analyzed by means of the FULLPROF program,[10] using the internal neutron-scattering lengths and the neutron magnetic form factor of Tb^{3+}.

III. CHEMICAL STRUCTURE

Figure 2 illustrates the neutron-diffraction pattern of $Tb_{14}Ag_{51}$ in the paramagnetic state at 300 K, which had been measured on HRPT in the high intensity mode with angular steps of 0.05°. As may be seen from the profile fit, it corresponds well to space group 175, $P6/m$ and the $Gd_{14}Ag_{51}$ structure.[1] 580 reflections (h,k,l) contribute to the pattern. For the mentioned space group there are no extinction rules, neither for the general positions nor for the special sites. Note in Fig. 2 also the large paramagnetic diffuse scattering from Tb^{3+} ions, increasing the background in particular at low scattering angles. At 30 K certain broad diffuse peaks due to short-range magnetic correlations are in addition visible at low scattering angles, in particular for $2\theta\approx 19.5°$, see the inset in Fig. 2. The refined structural parameters with atom designations similar to Ref. 4 are summarized in Table I for both 300 and 30 K. The room-temperature values are similar to those of $Gd_{14}Ag_{51}$.[1] In Table II the shortest interatomic Tb-Tb distances are given. They show the main Tb-Tb interactions and indicate essential frustrations. The shortest interatomic Tb distances are Tb3-Tb3 and Tb1-Tb1. The thermal contraction is anisotropic, predominantly parallel to the c axis. Within error limits the Tb1-Tb1 distance stays constant between 300 and 30 K, whereas Tb3-Tb3 shrinks essentially along the c axis. The characteristic sixfold rings of Tb1 and Tb2 are illustrated in Fig. 3. It furthermore illustrates possible frustrations in magnetic interactions.

IV. ANALYSIS OF MAGNETIC NEUTRON INTENSITIES

A. Determination of the propagation vector k

Long-range magnetic ordering yields in neutron-diffraction magnetic Bragg peaks which may be indexed as $\boldsymbol{\tau}\pm\mathbf{k}_j$, where $\boldsymbol{\tau}$ denotes in reciprocal space the position of a nuclear Bragg peak, and the propagation vectors $\mathbf{k}_j$ originate from a general Fourier expansion of the magnetic structure. Thus the first task in the determination of magnetic structures is to find the characteristic $\mathbf{k}$ vectors. Usually a single $\mathbf{k}$ vector is sufficient.[11]

Figure 4 shows the result of determining the propagation vector $\mathbf{k}=(1/3,1/3,0)$ by means of powder profile matching[10] of the magnetic neutron-difference pattern of $Tb_{14}Ag_{51}$: $I(1.5\text{ K})-I(30\text{ K})$. Apart from the small (1,0,0) peak, the pattern is well described ($\chi^2=20.8$, $R_{wp}=8.8\%$, $R_{exp}=1.9\%$, $R_{Bm}=0.1\%$) by $\mathbf{k}=(1/3,1/3,0)$ and $-\mathbf{k}$. The increase of the weak nuclear peak (1,0,0) is probably caused by a small $k=0$ magnetic-moment component.

Based on earlier DMC measurements with $\lambda=2.560$ Å on a stationary sample, the temperature dependences of charac-

TABLE I. Refined lattice parameters a, c, and atomic positional parameters of paramagnetic $Tb_{14}Ag_{51}$ at 300 and at 30 K for space group 175, $P6/m$, unit-cell volume $V=(\sqrt{3}/2)a^2c$, containing one formula unit Z. Estimated standard deviations of parameters are given within parentheses, refering to the last relevant digit. Isotropic temperature factor $B_{Tb}=0.81(3)$ Å^2, $B_{Ag}=0.86(3)$ Å^2 at 300 K, and overall temperature factor $B=0.0(1)$ Å^2 at 30 K. Agreement values (Ref. 10): Goodness of fit χ^2 and weighted R_{wp} factor concerning profile intensities, expected value R_{exp} according to counting statistics, and R_{Bn} concerning integrated nuclear intensities.

T (K)	a (Å)	c (Å)	χ^2	R_{wp} (%)	$R_{expt.}$	R_{Bn}
300	12.643(1)	9.296(1)	2.44	3.0	1.9	5.3
30	12.590(1)	9.267(1)	3.38	3.3	1.8	5.9
T (K)	Atom	Site	x	y	z	occup.
300	Tb1	6k	0.1411(3)	0.4694(3)	0.5	100
30			0.1433(2)	0.4703(2)		
300	Tb2	6j	0.3910(3)	0.1138(3)	0	100
30			0.3906(3)	0.1138(3)		
300	Tb3	2e	0	0	0.3069(6)	100
30					0.3104(5)	
300	Ag1	12l	0.0754(3)	0.2656(3)	0.2348(3)	100
30			0.0758(2)	0.2663(2)	0.2361(3)	
300	Ag2	12l	0.1161(3)	0.4935(3)	0.1527(3)	100
30			0.1166(2)	0.4943(2)	0.1522(3)	
300	Ag3	12l	0.4391(2)	0.1038(2)	0.3317(3)	100
30			0.4394(2)	0.1034(2)	0.3309(3)	
300	Ag4	6k	0.2388(3)	0.0608(4)	0.5	100
30			0.2378(3)	0.0588(4)		
300	Ag5	6j	−0.0057(7)	0.1204(8)	0	50[a]
30			−0.0018(6)	0.1225(7)		
300	Ag6	4h	1/3	2/3	0.2992(5)	100
30					0.2994(5)	
300	Ag7	2c	1/3	2/3	0	100
30					0	

[a]Nominal reduced occupation according to Ref. 4.

teristic magnetic Bragg peaks shown in Fig. 5 have been carefully determined. They prove the Néel temperature $T_N=27.5(5)$ K, in good agreement with the bulk magnetic measurements. The magnetic intensities decrease continuously with increase of the temperature, suggesting simultaneous magnetic ordering of the Tb sublattices and (apart from the weak 1,0,0 peak, which becomes significant only at lower temperatures) the absence of further magnetic phase transitions in the temperature range down to 1.5 K. Because of the probable influence of crystal-field effects on the ordered magnetic moments changing with temperature, we did not attempt any "Brillouin-type" fits to the measured points in Fig. 5.

B. Group theory analysis of magnetic symmetry in case of three magnetic A sublattices of a $A_{14}B_{51}$ chemical structure for k=(1/3,1/3,0)

The chemical structure of the $A_{14}B_{51}$ compound corresponds to space group 175, $P6/m$. Without proper symmetry analysis it is rather hopeless to determine from powder neutron-diffraction data the magnetic ordering in such a system with three magnetic A sublattices Tb1, Tb2, and Tb3

TABLE II. Shortest interatomic distances in $Tb_{14}Ag_{51}$, calculated by the program FULLPROF (Ref. 10). It should be noted that here the given error estimates correspond to two standard deviations to get more certain values.

Temperature/ Distance (Å)	300 K	30 K
Tb1—Tb1	4.01(1)	4.03(1)
	4.27(1)	4.215(8)
	5.27(1)	5.256(8)
Tb2—Tb1	5.221(6)	5.195(4)
	5.483(6)	5.477(4)
	5.752(6)	5.738(6)
Tb2—Tb2	4.41(1)	4.38(1)
	4.88(1)	4.87(1)
	5.53(1)	5.508(8)
Tb3—Tb1	5.571(8)	5.542(6)
Tb3—Tb2	5.248(8)	5.240(8)
Tb3—Tb3	3.59(2)	3.52(1)
	5.71(2)	5.75(1)

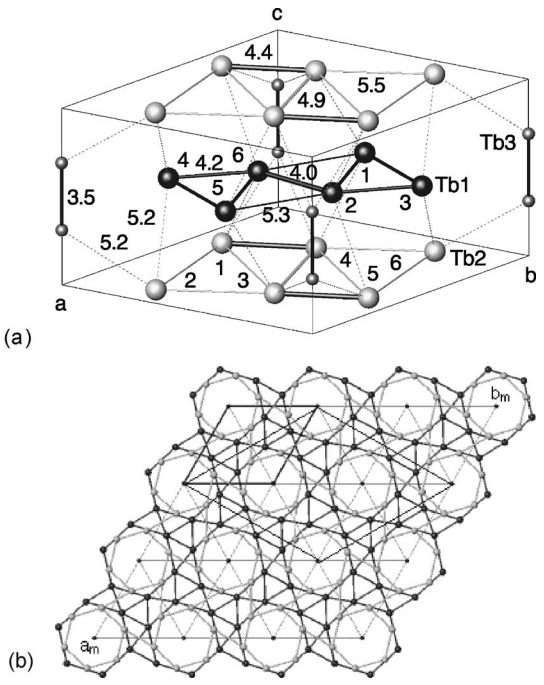

FIG. 3. (a) Tb sublattices of $Tb_{14}Ag_{51}$ with atom numbers according to Table I (30 K). The other numbers indicate characteristic interatomic distances, which imply considerable frustrations in magnetic interactions. Longer distances are shown as thinner lines. A chemical unit cell is outlined. (b) A view perpendicular to the c axis corresponding to the magnetic unit cell, with hexagonal Tb2 (inner, at $z=0$) and Tb1 (outer, at $z=1/2$) rings. Tb3 is shown with smaller diameter. With thick lines also the chemical unit cell is indicated. The unit cell based on the diagonal of the chemical cell represents a hexagonal H cell as the possible smallest magnetic unit cell.

according to the sites $(6k)$, $(6j)$, and $(2e)$, respectively (see Fig. 3). The chemical point symmetries of these sites are m, m, and 6, respectively. As only one magnetic transition is observed as a function of temperature, we may assume that all three magnetic sublattices order simultaneously according to the same irreducible representations. As explained by Izyumov and Naish,[11] magnetic ordering may usually be attributed to a specific propagation vector $\mathbf{k}$ and to a single irreducible representation τ_j of the space group of the chemical structure. Moreover, considering the magnetic moments as axial vectors, their generally complex Fourier components in the nth chemical unit cell are related to the ones in the "zero" cell by Eq. (1).

$$\mathbf{\Psi}_{jn} = \mathbf{\Psi}_{j0}\mathbf{e}^{i\varphi(n)}, \tag{1}$$

where $\varphi(n)=2\pi\mathbf{kt}$, and $\mathbf{t}(n)$ is a translation vector from the 0 cell to the n cell.

To obtain the real magnetic moments $\mathbf{S}(\mathbf{r}_j)$, one has to find suitable linear combinations, i.e., mixing coefficients of the basis vectors for $\mathbf{k}$ and $-\mathbf{k}$, respectively, making use of Eqs. (1) and (2).[12] This is equivalent to transformation from Fourier to direct space. For more details, see Ref. 12.

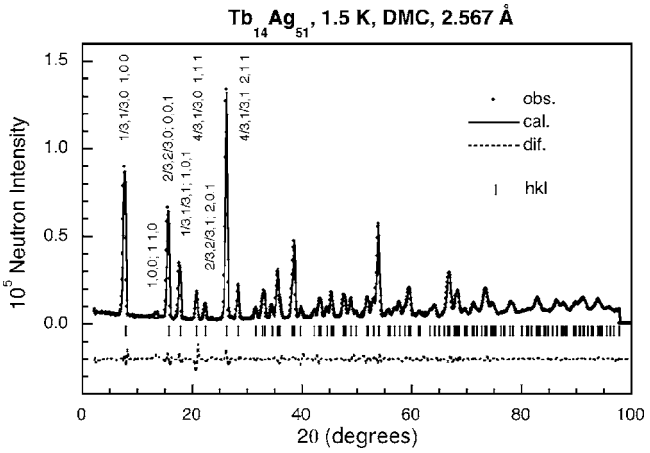

FIG. 4. Observed [points, magnetic difference intensities I{(1.5 K)−I(30 K)}, calculated (line, powder profile matching mode (Ref. 10) for $\mathbf{k}=(1/3,1/3,0)$ and $-\mathbf{k}$) as well as difference (dashed)] neutron-diffraction pattern of $Tb_{14}Ag_{51}$ at 1.5 K in the antiferromagnetic state. The alternative second indexing refers to a hexagonal H cell with lattice parameters $a_m=\sqrt{3}a$, $c_m=c$ of the smallest magnetic unit cell.

$$\mathbf{S}(\mathbf{r}_j) = \sum_{\mu,\nu,\lambda} c_{\mu\nu\lambda}\mathbf{\Psi}_{\mu\nu\lambda}(\mathbf{r}_j), \tag{2}$$

where μ labels arms of the star of $\mathbf{k}$, ν denotes the irreducible representations, and λ is the dimension of the representation. $\{\mathbf{r}_j\}$ refers to an orbit. These coefficients may be used as order parameters in the analysis of magnetic phase transitions.[12]

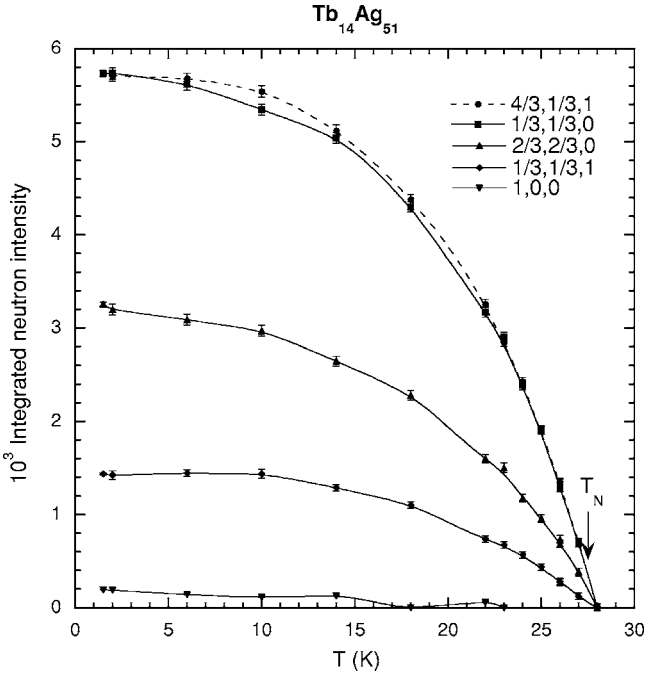

FIG. 5. Temperature dependences of the integrated magnetic neutron intensities of characteristic magnetic Bragg peaks of $Tb_{14}Ag_{51}$. The smooth curves are a guide to the eyes.

From neutron-diffraction results on $Tb_{14}Ag_{51}$ (see Fig. 4), we know $\mathbf{k}=(1/3,1/3,0)$. Based on the new Windows version of program MODY,[12] the corresponding basis vectors (magnetic modes ψ) are summarized in Table III for the three types of magnetic sites. The results were also checked by means of the program BASIREP.[10] The star of the vector $\mathbf{k}$ contains the two arms $\mathbf{k}_1=\mathbf{k}$ and $\mathbf{k}_2=(-1/3,2/3,0)$ which is equivalent to $-\mathbf{k}$. The propagation vector $\mathbf{k}$ [small group $G(\mathbf{k})$] implies a symmetry reduction to space group $P\bar{6}$ with symmetry elements 1, 3^+, 3^-, m, $\bar{6}^+$, and $\bar{6}^-$. For this case and space group $P6/m$, there are six one-dimensional irreducible representations τ_j (see Table III). The first two are real, and the other four are complex ($\tau_5=\tau_3^*, \tau_6=\tau_4^*$). Axial vector representations τ of the six magnetic moments with three components associated with both sites ($6k$) and ($6j$) decompose into two orbits of type $\tau=\tau_1+2\tau_2+\tau_3+2\tau_4+\tau_5+2\tau_6$. On the other hand, for sites ($2e$) only one orbit exits: $\tau=\tau_1+\tau_2+\tau_3+\tau_4+\tau_5+\tau_6$. Thus in the case of simultaneous magnetic ordering of all three sites, all τ_j are possible for each site. Furthermore, it should be noted that for the present space group (for irreducible representations τ_3, τ_4, τ_5, and τ_6 with Herring coefficient 0), one has to combine in the sense of a direct sum $\tau_3\oplus\tau_5$ magnetic modes (basis vectors) for $+\mathbf{k}$ from τ_3 with those for $-\mathbf{k}$ from τ_5 and vice versa (similar for $\tau_4\oplus\tau_6$).

With respect to possible magnetic configurations resulting from Table III, we summarize here only the needed results for the case of $\tau_4\oplus\tau_6$ which yielded the best fit of the measured neutron intensities of $Tb_{14}Ag_{51}$ at 1.5 K. For a more detailed discussion including other possibilities we refer the reader to Ref. 13, where the full symmetry analysis is explained.

For $\tau_4\oplus\tau_6$ the magnetic moments are restricted to the basal plane. It should be noted that the two orbits in the case of sites ($6k$) and ($6j$) are independent with respect to only symmetry considerations. This is indicated by different phases. Also the moment magnitudes could differ, but we consider this in view of probable exchange and dipolar interactions as less realistic.

One obtains (see Ref. 13) for sites ($6k$) cycloidal spiral solutions with constant magnitude of the magnetic Tb moments $\mathbf{S}_{jn}$ such as

$$\mathbf{S}_{1n}=S_1\{\mathbf{e}_x\cos[\varphi(n)+\alpha_1]+(1/\sqrt{3})(\mathbf{e}_x+2\mathbf{e}_y)\sin[\varphi(n)+\alpha_1]\},$$

$$\mathbf{S}_{2'n}=-S_1\{\mathbf{e}_y\cos[\varphi(n)+\pi/3+\alpha_1]-(1/\sqrt{3})(2\mathbf{e}_x+\mathbf{e}_y)\sin[\varphi(n)+\pi/3+\alpha_1]\},$$

$$\mathbf{S}_{3'n}=S_1\{(\mathbf{e}_x+\mathbf{e}_y)\cos[\varphi(n)-\pi/3+\alpha_1]-(1/\sqrt{3})(\mathbf{e}_x-\mathbf{e}_y)\sin[\varphi(n)-\pi/3+\alpha_1]\},$$

($6k46e$)

$$\mathbf{S}_{4'n}=S_1\{\mathbf{e}_x\cos[\varphi(n)+\beta_1]+(1/\sqrt{3})(\mathbf{e}_x+2\mathbf{e}_y)\sin[\varphi(n)+\beta_1]\},$$

$$\mathbf{S}_{5'n}=-S_1\{\mathbf{e}_y\cos[\varphi(n)+\pi/3+\beta_1]-(1/\sqrt{3})(2\mathbf{e}_x+\mathbf{e}_y)\sin[\varphi(n)+\pi/3+\beta_1]\},$$

$$\mathbf{S}_{6n}=S_1\{(\mathbf{e}_x+\mathbf{e}_y)\cos[\varphi(n)-\pi/3+\beta_1]-(1/\sqrt{3})(\mathbf{e}_x-\mathbf{e}_y)\sin[\varphi(n)-\pi/3+\beta_1]\},$$

where $\mathbf{e}_x$ and $\mathbf{e}_y$ are unit vectors along the basic translations $\mathbf{a}$ and $\mathbf{b}$, respectively. Configurations of the type ($6k46e$) with constant magnetic moment magnitude appear as reasonable with respect to the fact that the $4f$ electrons of heavy rare earths such as Tb^{3+} are generally rather well localized.

For the program FULLPROF,[10] the transformation matrices of magnetic moments are needed which are equivalent to relations such as ($6k46e$):

$$x,y,z:(u,v,w);\text{phase } 0,\quad -x,-y,z:(u,v,w);0,$$

($6k46f$)
$$-y,x-y,z:(v,-u+v,w);+\pi/3,$$
$$y,-x+y,z:(v,-u+v,w);+\pi/3,$$
$$-x+y,-x,z:(u-v,u,w);-\pi/3,$$
$$x-y,x,z:(u-v,u,w);-\pi/3.$$

It may be used both for modulated and constant magnitude configurations.

For sites ($6j$) the following relations were used in the 1.5-K refinement:

$$\mathbf{S}_{1n}=S_2\{\mathbf{e}_x\cos[\varphi(n)+\alpha_2]+(1/\sqrt{3})(\mathbf{e}_x+2\mathbf{e}_y)\sin[\varphi(n)+\alpha_2]\},$$

$$\mathbf{S}_{2'n}=-S_2\{\mathbf{e}_y\cos[\varphi(n)+\pi/3+\alpha_2]-(1/\sqrt{3})(2\mathbf{e}_x+\mathbf{e}_y)\sin[\varphi(n)+\pi/3+\alpha_2]\},$$

$$\mathbf{S}_{3'n}=S_2\{(\mathbf{e}_x+\mathbf{e}_y)\cos[\varphi(n)-\pi/3+\alpha_2]-(1/\sqrt{3})(\mathbf{e}_x-\mathbf{e}_y)\sin[\varphi(n)-\pi/3+\alpha_2]\},$$

($6j46e$)

$$\mathbf{S}_{4n}=S_2\{\mathbf{e}_x\cos[\varphi(n)+\beta_2]+(1/\sqrt{3})(\mathbf{e}_x+2\mathbf{e}_y)\sin[\varphi(n)+\beta_2]\},$$

$$\mathbf{S}_{5'n}=-S_2\{\mathbf{e}_y\cos[\varphi(n)+\pi/3+\beta_2]-(1/\sqrt{3})(2\mathbf{e}_x+\mathbf{e}_y)\sin[\varphi(n)+\pi/3+\beta_2]\},$$

$$\mathbf{S}_{6'n}=S_2\{(\mathbf{e}_x+\mathbf{e}_y)\cos[\varphi(n)-\pi/3+\beta_2]-(1/\sqrt{3})(\mathbf{e}_x-\mathbf{e}_y)\sin[\varphi(n)-\pi/3+\beta_2]\},$$

$$x,y,z:(u,v,w);\text{phase } 0,\quad -x,-y,z:(u,v,w);0,$$

($6j46f$)
$$-y,x-y,z:(v,-u+v,w);+\pi/3,$$
$$y,-x+y,z:(v,-u+v,w);+\pi/3,$$
$$-x+y,-x,z:(u-v,u,w);-\pi/3,$$

TABLE III. Irreducible representations and magnetic modes ψ (Ref. 12) for space group $P6/m$, 175, $\mathbf{k}=\pm(1/3,1/3,0)$ and sites (6*k*), (6*j*), and (2*e*). $a=e^{i\pi/3}$, $b=e^{i\pi/6}$. Within parentheses the mode components along the basic translations of the chemical unit cell are given. With respect to magnetic neutron intensity calculations, it is for the present hexagonal symmetry in the case of sites (6*k*) and (6*j*) more convenient to use instead of the magnetic atoms in the chemical unit cell (atoms designated without primes, see also Fig. 3) atom positions centered around the origin (marked by $'$), making use of Eq. (1).

Sym. op./ Irred. rep.	1	3^+	3^-	$\bar{6}^+$	m	$\bar{6}^-$
τ_1	1	1	1	1	1	1
τ_2	1	1	1	−1	−1	−1
τ_3	1	$-a^*$	$-a$	1	$-a^*$	$-a$
τ_4	1	$-a^*$	$-a$	−1	a^*	a
τ_5	1	$-a$	$-a^*$	1	$-a$	$-a^*$
τ_6	1	$-a$	$-a^*$	−1	a	a^*
			(6*k*):			
		$2=2'+(1,1,0),3=3'+(0,1,0),4=4'+(1,0,0),5=5'+(1,1,0)$				
Atom	1:	2′:	3′:	4′:	5′:	6:
Position	x,y,z	$-y,x-y,z$	$-x+y,-x,z$	$x-y,x,z$	$-x,-y,z$	$y,-x+y,z$
Orbit	1	1	1	2	2	2
$\psi_{6k}(\tau_1,\mathbf{k})$	(0,0,1)	(0,0,1)	(0,0,1)	$(0,0,-a)$	$(0,0,-a)$	$(0,0,-a)$
$\psi_{6k}(\tau_1,-\mathbf{k})$	$(0,0,-a)$	$(0,0,-a)$	$(0,0,-a)$	(0,0,1)	(0,0,1)	(0,0,1)
$\psi_{a,6k}(\tau_2,\mathbf{k})$	(1,0,0)	(0,1,0)	(−1,−1,0)	$(-a,0,0)$	$(0,-a,0)$	$(a,a,0)$
$\psi_{a,6k}(\tau_2,-\mathbf{k})$	$(0,a,0)$	$(-a,-a,0)$	$(a,0,0)$	(1,1,0)	(−1,0,0)	(0,−1,0)
$\psi_{b,6k}(\tau_2,\mathbf{k})$	(0,1,0)	(−1,−1,0)	(1,0,0)	$(0,-a,0)$	$(a,a,0)$	$(-a,0,0)$
$\psi_{b,6k}(\tau_2,-\mathbf{k})$	$(-a,-a,0)$	$(a,0,0)$	$(0,a,0)$	(−1,0,0)	(0,−1,0)	(1,1,0)
$\psi_{6k}(\tau_3,\mathbf{k})$	(0,0,1)	$(0,0,-a)$	$(0,0,-a^*)$	$(0,0,-a)$	$(0,0,-a^*)$	(0,0,1)
$\psi_{6k}(\tau_3,-\mathbf{k})$	(0,0,1)	$(0,0,-a)$	$(0,0,-a^*)$	(0,0,1)	$(0,0,-a)$	$(0,0,-a^*)$
$\psi_{a,6k}(\tau_4,\mathbf{k})$	(1,0,0)	$(0,-a,0)$	$(a^*,a^*,0)$	$(-a,0,0)$	$(0,-a^*,0)$	(−1,−1,0)
$\psi_{a,6k}(\tau_4,-\mathbf{k})$	(0,−1,0)	$(-a,-a,0)$	$(a^*,0,0)$	(1,1,0)	$(a,0,0)$	$(0,a^*,0)$
$\psi_{b,6k}(\tau_4,\mathbf{k})$	(0,1,0)	$(a,a,0)$	$(-a^*,0,0)$	$(0,-a,0)$	$(a^*,a^*,0)$	(1,0,0)
$\psi_{b,6k}(\tau_4,-\mathbf{k})$	(1,1,0)	$(a,0,0)$	$(0,a^*,0)$	(−1,0,0)	$(0,a,0)$	$(-a^*,-a^*,0)$
$\psi_{6k}(\tau_5,\mathbf{k})$	(0,0,1)	$(0,0,-a^*)$	$(0,0,-a)$	$(0,0,-a)$	(0,0,1)	$(0,0,-a^*)$
$\psi_{6k}(\tau_5,-\mathbf{k})$	$(0,0,-a^*)$	$(0,0,-a)$	(0,0,1)	(0,0,1)	$(0,0,-a^*)$	$(0,0,-a)$
$\psi_{a,6k}(\tau_6,\mathbf{k})$	(1,0,0)	$(0,-a^*,0)$	$(a,a,0)$	$(-a,0,0)$	(0,1,0)	$(a^*,a^*,0)$
$\psi_{a,6k}(\tau_6,-\mathbf{k})$	$(0,a^*,0)$	$(-a,-a,0)$	(−1,0,0)	(1,1,0)	$(a^*,0,0)$	$(0,a,0)$
$\psi_{b,6k}(\tau_6,\mathbf{k})$	(0,1,0)	$(a^*,a^*,0)$	$(-a,0,0)$	$(0,-a,0)$	(−1,−1,0)	$(-a^*,0,0)$
$\psi_{b,6k}(\tau_6,-\mathbf{k})$	$(-a^*,-a^*,0)$	$(a,0,0)$	(0,−1,0)	(−1,0,0)	$(0,a^*,0)$	$(-a,-a,0)$
			(6*j*):			
		$2=2'+(1,0,0),3=3'+(1,1,0),5=5'+(1,1,0),6=6'+(0,1,0)$				
Atom	1:	2′:	3′:	4:	5′:	6′:
Position	x,y,z	$-y,x-y,z$	$-x+y,-x,z$	$x-y,x,z$	$-x,-y,z$	$y,-x+y,z$
Orbit	1	1	1	2	2	2
$\psi_{6j}(\tau_1,\mathbf{k})$	(0,0,1)	(0,0,1)	(0,0,1)	(0,0,1)	(0,0,1)	(0,0,1)
$\psi_{6j}(\tau_1,-\mathbf{k})$	(0,0,1)	(0,0,1)	(0,0,1)	(0,0,1)	(0,0,1)	(0,0,1)
$\psi_{a,6j}(\tau_2,\mathbf{k})$	(1,0,0)	(0,1,0)	(−1,−1,0)	(1,0,0)	(0,1,0)	(−1,−1,0)
$\psi_{a,6j}(\tau_2,-\mathbf{k})$	(0,−1,0)	(1,1,0)	(−1,0,0)	(1,1,0)	(−1,0,0)	(0,−1,0)
$\psi_{b,6j}(\tau_2,\mathbf{k})$	(0,1,0)	(−1,−1,0)	(1,0,0)	(0,1,0)	(−1,−1,0)	(1,0,0)
$\psi_{b,6j}(\tau_2,-\mathbf{k})$	(1,1,0)	(−1,0,0)	(0,−1,0)	(−1,0,0)	(0,−1,0)	(1,1,0)
$\psi_{6j}(\tau_3,\mathbf{k})$	(0,0,1)	$(0,0,-a)$	$(0,0,-a^*)$	(0,0,1)	$(0,0,-a)$	$(0,0,-a^*)$
$\psi_{6j}(\tau_3,-\mathbf{k})$	$(0,0,-a^*)$	(0,0,1)	$(0,0,-a)$	(0,0,1)	$(0,0,-a)$	$(0,0-a^*)$
$\psi_{a,6j}(\tau_4,\mathbf{k})$	(1,0,0)	$(0,-a,0)$	$(a^*,a^*,0)$	(1,0,0)	$(0,-a,0)$	$(a^*,a^*,0)$
$\psi_{a,6j}(\tau_4,-\mathbf{k})$	$(0,a^*,0)$	(1,1,0)	$(a,00)$	(1,1,0)	$(a,0,0)$	$(0,a^*,0)$

TABLE III. (*Continued.*)

Sym. op./ Irred. rep.	1	3^+	3^-	$\bar{6}^+$	m	$\bar{6}^-$
$\psi_{b,6j}(\tau_4,\mathbf{k})$	(0,1,0)	$(a,a,0)$	$(-a^*,0,0)$	(0,1,0)	$(a,a,0)$	$(-a^*,0,0)$
$\psi_{b,6j}(\tau_4,-\mathbf{k})$	$(-a^*,-a^*,0)$	$(-1,0,0)$	$(0,a,0)$	$(-1,0,0)$	$(0,a,0)$	$(-a^*,-a^*,0)$
$\psi_{6j}(\tau_5,\mathbf{k})$	(0,0,1)	$(0,0,-a^*)$	$(0,0,-a)$	(0,0,1)	$(0,0,-a^*)$	$(0,0,-a)$
$\psi_{6j}(\tau_5,-\mathbf{k})$	$(0,0,-a)$	(0,0,1)	$(0,0,-a^*)$	(0,0,1)	$(0,0,-a^*)$	$(0,0,-a)$
$\psi_{a,6j}(\tau_6,\mathbf{k})$	(1,0,0)	$(0,-a^*,0)$	$(a,a,0)$	(1,0,0)	$(0,-a^*,0)$	$(a,a,0)$
$\psi_{a,6j}(\tau_6,-\mathbf{k})$	$(0,a,0)$	(1,1,0)	$(a^*,0,0)$	(1,1,0)	$(a^*,0,0)$	$(0,a,0)$
$\psi_{b,6j}(\tau_6,\mathbf{k})$	(0,1,0)	$(a^*,a^*,0)$	$(-a,0,0)$	(0,1,0)	$(a^*,a^*,0)$	$(-a,0,0)$
$\psi_{b,6j}(\tau_6,-\mathbf{k})$	$(-a,-a,0)$	$(-1,0,0)$	$(0,a^*,0)$	$(-1,0,0)$	$(0,a^*,0)$	$(-a,-a,0)$
	$(2e)$:					
Atom	1:	2:				
Position	$0,0,z$	$0,0,1-z$				
Orbit	1	1				
$\psi_{2e}(\tau_1,\mathbf{k})$	(0,0,1)	(0,0,1)				
$\psi_{2e}(\tau_1,-\mathbf{k})$	(0,0,1)	(0,0,1)				
$\psi_{2e}(\tau_2,\mathbf{k})$	(0,0,1)	$(0,0,-1)$				
$\psi_{2e}(\tau_2,-\mathbf{k})$	(0,0,1)	$(0,0,-1)$				
$\psi_{2e}(\tau_3,\mathbf{k})$	$(b^*,-i,0)/\sqrt{3}$	$-(b^*,-i,0)/\sqrt{3}$				
$\psi_{2e}(\tau_3,-\mathbf{k})$	$(b,b^*,0)/\sqrt{3}$	$-(b,b^*,0)/\sqrt{3}$				
$\psi_{2e}(\tau_4,\mathbf{k})$	$(b^*,-i,0)/\sqrt{3}$	$(b^*,-i,0)/\sqrt{3}$				
$\psi_{2e}(\tau_4,-\mathbf{k})$	$(b,b^*,0)/\sqrt{3}$	$(b,b^*,0)/\sqrt{3}$				
$\psi_{2e}(\tau_5,\mathbf{k})$	$(b,i,0)/\sqrt{3}$	$-(b,i,0)/\sqrt{3}$				
$\psi_{2e}(\tau_5,-\mathbf{k})$	$(b^*,b,0)/\sqrt{3}$	$-(b^*,b,0)/\sqrt{3}$				
$\psi_{2e}(\tau_6,\mathbf{k})$	$(b,i,0)/\sqrt{3}$	$(b,i,0)/\sqrt{3}$				
$\psi_{2e}(\tau_6,-\mathbf{k})$	$(b^*,b,0)/\sqrt{3}$	$(b^*,b,0)/\sqrt{3}$				

$$x-y,x,z:(u-v,u,w);-\pi/3,$$

$$\mathbf{S}_{1n}=S_2\{\mathbf{e}_x\cos[\varphi(n)+\alpha_2]+(1/\sqrt{3})(\mathbf{e}_x+2\mathbf{e}_y)\sin[\varphi(n)+\alpha_2]\},$$

$$\mathbf{S}_{2'n}=-S_2\{\mathbf{e}_y\cos[\varphi(n)-\pi/3+\alpha_2]-(1/\sqrt{3})(2\mathbf{e}_x+\mathbf{e}_y)\sin[\varphi(n)-\pi/3+\alpha_2]\},$$

$$\mathbf{S}_{3'n}=S_2\{(\mathbf{e}_x+\mathbf{e}_y)\cos[\varphi(n)+\pi/3+\alpha_2]-(1/\sqrt{3})(\mathbf{e}_x-\mathbf{e}_y)\sin[\varphi(n)+\pi/3+\alpha_2]\},$$

$(6j46e')$

$$\mathbf{S}_{4n}=S_2\{\mathbf{e}_x\cos[\varphi(n)+\beta_2]+(1/\sqrt{3})(\mathbf{e}_x+2\mathbf{e}_y)\sin[\varphi(n)+\beta_2]\},$$

$$\mathbf{S}_{5'n}=-S_2\{\mathbf{e}_y\cos[\varphi(n)-\pi/3+\beta_2]-(1/\sqrt{3})(2\mathbf{e}_x+\mathbf{e}_y)\sin[\varphi(n)-\pi/3+\beta_2]\},$$

$$\mathbf{S}_{6'n}=S_2\{(\mathbf{e}_x+\mathbf{e}_y)\cos[\varphi(n)+\pi/3+\beta_2]-(1/\sqrt{3})(\mathbf{e}_x-\mathbf{e}_y)\sin[\varphi(n)+\pi/3+\beta_2]\},$$

$$x,y,z:(u,v,w);0,\quad -x,-y,z:(u,v,w);0,$$

$$(6j46f')\quad -y,x-y,z:(v,-u+v,w);-\pi/3,$$

$$y,-x+y,z:(v,-u+v,w);-\pi/3,$$

$$-x+y,-x,z:(u-v,u,w);+\pi/3,$$

$$x-y,x,z:(u-v,u,w);+\pi/3$$

Concerning the third kind of sites $(2e)$ results for $\tau_4\oplus\tau_6$:

$$(2e46)\ \mathbf{S}_{1n}=S_3\{\mathbf{e}_x\cos[\varphi(n)+\alpha_3]+(1/\sqrt{3})(\mathbf{e}_x+2\mathbf{e}_y)\sin[\varphi(n)+\alpha_3]\}=\mathbf{S}_{2n}.$$

As the cosine and sine terms correspond to perpendicular directions, one thus again obtains the possibility of a triangular moment configuration in the basal plane with constant magnitude of the magnetic moments.

Reference 13 discussed, in more detail, magnetic configurations showing that the particular **k** vector implies in a natural way a decomposition into three magnetic sublattices A, B, and C, either by 120° rotations in the case of planar models or by characteristic phase shifts for amplitude modulation. Thus one may choose a hexagonal H cell as the smallest magnetic unit cell, but for convenience we compare it to the chemical unit cell along the **a**- and **b**-direction tripled magnetic unit cell. As in this cell translations 0,0,0; 2/3,1/3,0 and 1/3,2/3,0 belong to the same sublattice, one obtains the rule $-h+k=3n$, n=integer for allowed magnetic peaks.

Finally we would like to mention that a similar symmetry analysis for $k=0$ shows that the $U_{14}Au_{51}$ magnetic structure[4] corresponds to the real irreducible representation τ_2.

C. Profile fitting of magnetic neutron intensities of $Tb_{14}Ag_{51}$

With the models of magnetic ordering derived in Ref. 13 and in particular with the equations summarized in the previous section, we performed FULLPROF (Ref. 10) refinements. For this purpose we combined in a two-pattern calculation with equal weights the 1.5-K data with sample oscillation of $Tb_{14}Ag_{51}$ from DMC (2.567 Å, scattering angle step 0.1°, 979 data points) and HRPT (1.886 Å, step 0.05°, 3208 data points). Whereas the DMC data have higher counting statistics and are dominated by magnetic neutron intensities, the latter are almost negligible in the high angle part of the HRPT data. Thus in principle it would be possible to determine also structural changes induced by magnetic ordering. In order to avoid too many parameters, we used a polynomial fit of the background of the two patterns (six parameters per pattern). We excluded the first magnetic peak of the HRPT data because of difficulties to properly model the asymmetry correction and steep increase of the background at low angles. For the chemical structure we started from the positional parameters obtained in the paramagnetic state at 30 K. We refined it in an iterative way, starting with approximate values for instrumental and background parameters and first varied mainly magnetic-moment magnitudes and corresponding phases. Best agreement between observed and calculated magnetic neutron intensities and reasonable magnitudes of ordered magnetic moments were finally obtained for the combined irreducible representations τ_4 and τ_6 (direct sum $\tau_4 \oplus \tau_6$) according to the equation ($6k46f$) for both orbits of Tb1, ($6j46f'$) for orbit 1 and ($6j46f$) for orbit 2 of Tb2 and ($2e46$) for Tb3, see Ref. 13. This is equivalent to the combination of ($6k46e$) for both orbits of Tb1, ($6j46e'$) for orbit 1 and ($6j46e$) for orbit 2 of Tb2 and ($2e46$) for Tb3.[13] With the structural parameters taken from the 30-K values of Table I, 37 parameters were refined, yielding the agreement values $\chi_1^2=258$, $R_{wp}=10.9\%$, $R_{exp}=0.7\%$, $R_{Bn}=6.8\%$ (nuclear), $R_{Bm}=13.6\%$ (magnetic) for the DMC data and $\chi_2^2=22$, $R_{wp}=8.0\%$,$R_{exp}=1.7\%$, $R_{Bn}=5.6\%$, $R_{Bm}=12.6\%$ for the HRPT data. The determined ordered magnetic moments at 1.5 K are $\mu_{Tb1}=8.6(1)\mu_B$, $\mu_{Tb2}=8.2(1)\mu_B$, $\mu_{Tb3}=7.4(3)\mu_B$ and the free phases in units of 2π are $\alpha_1=0$ (fixed), $\beta_1=0.429(5)$, $\alpha_2=0.4(2)$, $\beta_2=0.51(1)$, and $\alpha_3=0.30(1)$. These fits are illustrated in Fig. 6. Finally the structural parameters were refined too, resulting in altogether 56 parameters. As, however, the improvements were only marginal ($\chi_1^2=239$, $\chi_2^2=24$), combined with rather large errors of the structural parameters, we finally kept the atomic parameters as determined for 30 K.

In view of the complexity of the chemical and magnetic structures of $Tb_{14}Ag_{51}$, the attained fit appears to be reasonable, although similar smaller deviations in both patterns at lower scattering angles indicate limitations of the derived magnetic ordering.

The slight increase of the weak peaks (1,0,0) and (2,0,0) in the magnetically ordered state may be best explained by assuming a ferromagnetic $k=0$ component for Tb3 along the c direction according to the irreducible representation τ_1, yielding a magnitude of approximately $2.6(3)\mu_B$ per Tb at 1.5 K. The corresponding decrease of χ^2 is only marginal. Thus this model is not unambiguous. It should be checked by further single-crystal studies. The resulting cycloidal magnetic spiral or triangular structure with the Tb magnetic moments in the (a,b) plane (neglecting the possible $k=0$ contribution) is illustrated in Fig. 7.

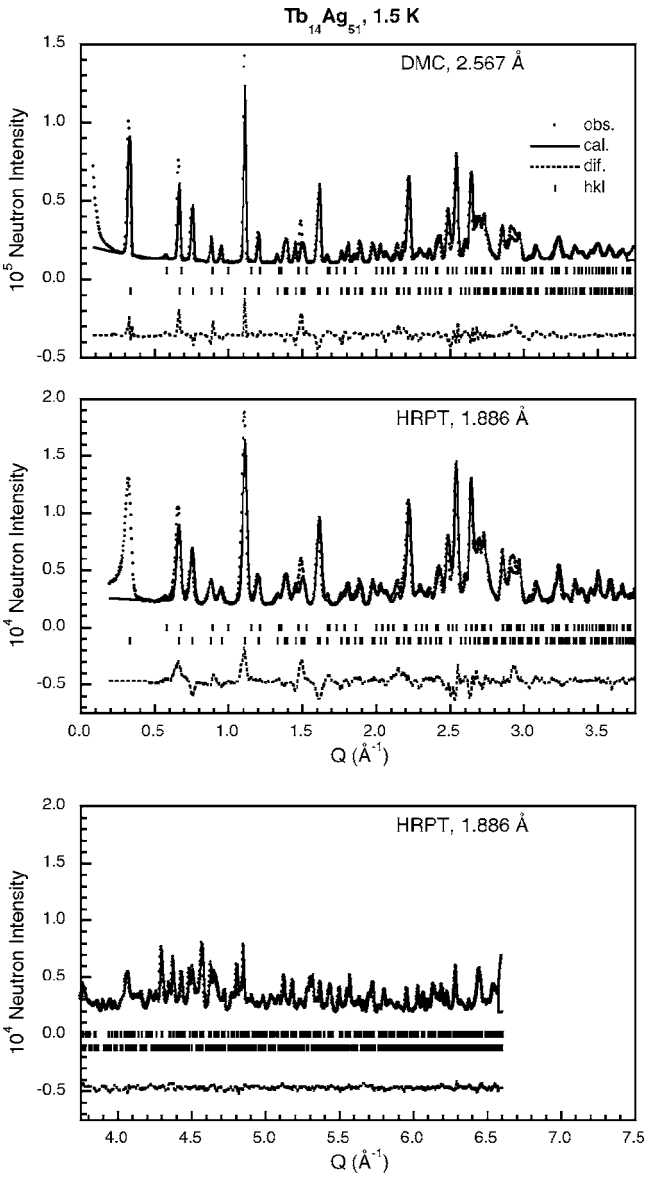

FIG. 6. Observed (from DMC and from HRPT, respectively), calculated and difference neutron-diffraction patterns of $Tb_{14}Ag_{51}$ at 1.5 K versus momentum transfer $Q=(4\pi \sin\theta/\lambda)$, for better comparison. Vertical bars indicate Bragg peak positions (nuclear upper and magnetic lower).

V. DISCUSSION AND CONCLUSIONS

Bulk magnetic, x-ray, and neutron-diffraction measurements were performed on $Tb_{14}Ag_{51}$ in the temperature range

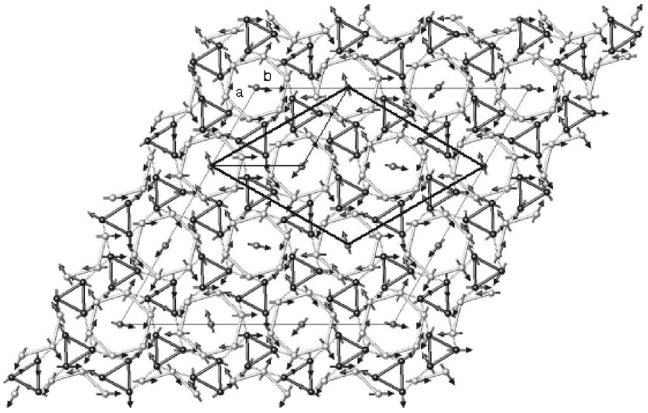

FIG. 7. Projection of the magnetic structure of $Tb_{14}Ag_{51}$ at 1.5 K onto the basal plane. The conventional magnetic unit cell outlined in grey contains 126 Tb atoms. Tb1, Tb2, and Tb3 are shown by black, grey, and darker grey colors, respectively. Also a chemical unit cell and a smallest magnetic hexagonal H unit cell are indicated by thin and thicker black lines, respectively.

from 1.5 K to room temperature. In the present x-ray and powder neutron-diffraction measurements on $Tb_{14}Ag_{51}$, its chemical structure in the paramagnetic state has been shown to correspond well to the $Gd_{14}Ag_{51}$ type[1] with space group $P6/m$. The structural parameters have been refined precisely both at 300 and at 30 K from the HRPT data. The measured bulk magnetic properties indicate antiferromagnetic Tb^{3+} ordering of $Tb_{14}Ag_{51}$ below $T_N=(27-27.9)$ K.

Combined with a thorough group-theoretical symmetry analysis, we show by means of neutron diffraction that the magnetic structure of this intermetallic compound is of a different $\mathbf{k}=(1/3,1/3,0)$ type, where all three magnetic Tb sublattices order simultaneously below $T_N=27.5(5)$ K. The magnetic Tb ordering of $Tb_{14}Ag_{51}$ corresponds in the sense of a direct sum $\tau_4 \oplus \tau_3$ to the combined irreducible representations τ_4 and τ_6. At 1.5 K the ordered magnetic Tb1 moment attains almost the free ion value of $9\mu_B$ of Tb^{3+} [refined value $8.6(1)\mu_B$]. On the other hand, the ordered magnetic moments of Tb2: $8.2(1)\mu_B$ and of Tb3: $7.4(3)\mu_B$ are somewhat lower, presumably due to crystal-field and frustration effects. According to cycloidal spiral, respectively, triangular configurations, the magnetic Tb moments are oriented parallel to the hexagonal (a,b) plane, see Fig. 7. Tb3 ions (sublattice A) are at the corners of a hexagonal H cell. Parallel to the b axis the other two Tb3 atoms in this magnetic cell are turned by 120° and 240°, respectively (sublattices B and C). The characteristic Tb1 triangles shown in Fig. 7 indicate considerable frustrations in the magnetic interactions. They are presumably also the reason for the rather low symmetry of the determined magnetic ordering of $Tb_{14}Ag_{51}$. In the hexagon of Tb1 around the center axis containing Tb3, the two orbits containing each three parallel moments of largest magnitude, are almost oriented antiparallel. For dominant antiferromagnetic intraexchange interaction J_1 this would be a energetically favorable configuration of the Tb1 hexagon. In case of the Tb2 hexagon the magnetic field at the Tb3 sites is determined by the three parallel moments of the Tb2b orbit. Thus the magnetic fields at the Tb3 sites do not vanish, in contrast to $U_{14}Au_{51}$.[4,5] This is consistent with magnetic order also on the Tb3 sublattice. As the latter ordering is antiferromagnetic, depending on the internal magnetic field, the magnetic moments may deviate in orientation from the magnetic-field direction. In summary, for $A_{14}B_{51}$ compounds a different type of $\mathbf{k}=(1/3,1/3,0)$ magnetic configuration with constant magnitudes of the magnetic moments has been determined for $Tb_{14}Ag_{51}$. As the $4f$ electrons of Tb^{3+} may be considered well localized in this compound, modulated structures appear as less probable than constant magnetic-moment configurations. The present conclusions on the rather complex magnetic ordering of $Tb_{14}Ag_{51}$ should be considered as important results, which with respect to certain details may be improved by further single-crystal studies. In particular it should be investigated to which extent the observed slight increase of weak nuclear peaks such as (1,0,0) in the magnetically ordered state is intrinsic to this material. These neutron intensity changes may be due to a small ferromagnetic moment component associated with $k=0$.

Presumably because of the lower Néel temperature of 22 K, differences in exchange interactions and geometrical frustrations, due to the less localized $5f$ electrons, the antiferromagnetic ordering of $k=0$ type holds for the heavy-fermion compound $U_{14}Au_{51}$,[4,5] and only the U1 and U2 sublattices have magnetic moments of $2.2\mu_B$ and $1.4\mu_B$, respectively. It should be interesting to extend bulk magnetic, neutron-diffraction studies, in particular also zero-field polarimetry measurements, as well as μSR investigations on single crystals, in this fascinating class of magnetic $A_{14}B_{51}$ materials. In particular it would be worthwhile to perform such investigations on the heavy-fermion compounds $Ce_{14}X_{51}$,[2] with less localized $4f$ electrons.

ACKNOWLEDGMENTS

Main parts of this work were performed at the Swiss spallation neutron source SINQ and on μSR facilities of the Paul Scherrer Institute, CH-5232 Villigen PSI. One of us (P.F.) thanks the Laboratory for Neutron Scattering of ETHZ and PSI for the provided SINQ test time and support. V.P. acknowledges μSR test time. W.S. is grateful to the State Committee for Scientific Research in Poland for financial support. The authors also thank Professor S. Maleyev from St. Peterburg Nuclear Physics Institute, Gatchina for clarifying theory discussions with respect to magnetic ordering determined in the present investigation.

*Corresponding author. Fax: +41564440750. Email address: Peter.Fischer@psi.ch
†Present address: NTB, CH-9470 Buchs, Switzerland

[1] D. M. Bailey and G. R. Kline, Acta Crystallogr., Sect. B: Struct. Crystallogr. Cryst. Chem. **27**, 650 (1971).
[2] O. Trovarelli, P. Stickar, J. G. Sereni, G. Schmerber, and J. P. Kappler, Solid State Commun. **89**, 421 (1994).
[3] A. Dommann, H. R. Ott, F. Hulliger, and P. Fischer, J. Less-Common Met. **160**, 171 (1990).
[4] P. J. Brown, J. Crangle, K.-U. Neumann, J. G. Smith, and K. R. A. Ziebeck, J. Phys.: Condens. Matter **9**, 4729 (1997).
[5] A. Schenck, M. Pinkpank, F. N. Gygax, K.-U. Neumann, K. R. A. Ziebeck, and A. Amato, J. Phys.: Condens. Matter **10**, 8059 (1998).
[6] A. Dommann, P. Fischer, and F. Hulliger, Progress report neutron scattering LNS-154, 60 (1991).
[7] H. R. Ott, E. Felder, A. Schilling, A. Dommann, and F. Hulliger, Solid State Commun. **71**, 549 (1989).
[8] P. Fischer, L. Keller, J. Schefer, and J. Kohlbrecher, Neutron News **11**(3), 19 (2000).
[9] P. Fischer, G. Frey, M. Koch, M. Könnecke, V. Pomjakushin, J. Schefer, R. Thut, N. Schlumpf, R. Bürge, U. Greuter, S. Bondt, and E. Berruyer, Physica B **276–278**, 146 (2000).
[10] J. Rodriguez-Carvajal, Physica B **192**, 55 (1993).
[11] Yu. A. Izyumov and V. E. Naish, J. Magn. Magn. Mater. **12**, 239 (1979).
[12] W. Sikora, F. Bialas, and L. Pytlik, J. Appl. Crystallogr. **37**, 1015 (2004).
[13] P. Fischer, V. Pomjakushin, L. Keller, A. Daoud-Aladine, W. Sikora, A. Dommann, and F. Hulliger, cond-mat/0506249 (unpublished).